applied sciences

MDPI

Article

Investigation of Energy Harvesting Capabilities of Metglas 2605SA1

Yuanyuan Liu [1,2,3], Benjamin Ducharne [3], Gaël Sebald [3], Kanjuro Makihara [2] and Mickaël Lallart [1,*]

[1] Univ. Lyon, INSA-Lyon, LGEF EA682, F-69621 Villeurbanne, France
[2] Department of Aerospace Engineering, Tohoku University, Sendai 980-8579, Japan
[3] ELyTMaX UMI 3757, CNRS, Univ. Lyon, INSA Lyon, Centrale Lyon, Université Claude Bernard Lyon 1, Tohoku University, Sendai 980-8577, Japan
* Correspondence: mickael.lallart@insa-lyon.fr

Abstract: In the framework of electromechanical energy conversion devices for vibrational energy harvesting, magnetostrictive materials are an attractive alternative solution to the brittleness of piezoelectric materials. Electromagnetic systems have low voltage output at a low frequency while magnetostrictive materials are suitable for a larger frequency bandwidth. In this work, a special experimental emphasis is placed on $Fe_{80}Si_9B_{11}$ (also known as Metglas 2605SA1) alloy. The ultimate energy conversion abilities are investigated by performing experimental Ericsson cycles as well as through theoretical predictions using a dedicated model for the magnetic curves at the material scale. Typical output magnetic energy densities ranged between 0.1 and 1 mJ/cm^3/cycle under moderate stress (<100 MPa) and magnetic excitation (up to 4 kA/m). Apart from its energy conversion abilities, Metglas 2605SA1 also features attractive characteristics for realistic applications in microgenerators, such as a low price, which is an important advantage for the mass production and cost-effectiveness of the harvester. Furthermore, its soft magnetic property reduces the need for high magnetic fields and yields a well-adapted solution from a system point of view. It is therefore shown that this material is a suitable conversion material according to the available stress and magnetic excitation magnitudes, in addition to economic considerations.

Keywords: energy harvesting; magnetostrictive; Metglas 2605SA1; Ericsson cycle

check for updates

Citation: Liu, Y.; Ducharne, B.; Sebald, G.; Makihara, K.; Lallart, M. Investigation of Energy Harvesting Capabilities of Metglas 2605SA1. *Appl. Sci.* **2023**, *13*, 3477. https://doi.org/10.3390/app13063477

Academic Editor: Alessandro Lo Schiavo

Received: 8 February 2023
Revised: 4 March 2023
Accepted: 6 March 2023
Published: 9 March 2023

Copyright: © 2023 by the authors. Licensee MDPI, Basel, Switzerland. This article is an open access article distributed under the terms and conditions of the Creative Commons Attribution (CC BY) license (https://creativecommons.org/licenses/by/4.0/).

1. Introduction

The number of wireless sensors and sensor networks is increasing with the rapid growth of the Internet of Things [1]. Powering such devices typically relies on primary batteries, leading to a short lifespan due to self-discharge, for instance [2], which becomes even more critical than the actual used energy. In this framework, energy harvesting systems are a great alternative to batteries and their associated drawbacks, such as environmental concerns, in the framework of self-powered sensors and sensor networks [3]. The harvester could be classified according to the energy source [4] and corresponding conversion material, such as magnetostrictive alloys for vibrational sources, thermoelectric modules for thermal energy [5,6], and photovoltaic cells for solar sources [7]. Among the available energy sources, vibrations remain one of the most attractive options due to their ubiquity, availability even in confined environments, and good power densities [8]. A complete electromechanical energy harvesting system [9] consists of three main components: conversion material [10], mechanical structure [11,12], and electrical interface [13].

From the conversion material [14] point of view, most of the existing vibrational energy harvesters use piezoelectric, magnetodynamic, or magnetostrictive coupling [15]. Piezoelectric materials are interesting because of their significant voltage output and active nature, but they also show several disadvantages such as potentially high voltage, low current, and high impedance at low frequency, typical to vibrational systems [16]. On the other

hand, magnetodynamic systems show several shortcomings such as low voltage output and predominant resistive losses at low frequencies. Magnetostrictive materials allow addressing such issues due to stress-dependent magnetic characteristics. The solid-state aspect of the magnetomechanical coupling in magnetostrictive materials also yields more compact devices compared to magnetodynamic systems, as the latter requires significant dimensional changes to allow the conversion to take place.

Joule discovered the effect of magnetostriction in 1842 [17], consisting of a change in the sample shape when subjected to a magnetic field. Villari [18] observed the inverse magnetostrictive effect, where the sample magnetization changes when mechanical stresses are applied to it. Energy harvesting systems using magnetostrictive materials exploit the Villari effect [19] and convert the variation of the mechanical excitation during vibration into a change in magnetic flux density, therefore inducing currents in the coils around the specimen.

The magnetization of ferromagnetic material in response to an applied magnetic field originates from two related mechanisms [20]: the domain wall motions, and the rotation of magnetic moments within domains towards the field direction. The effect of magnetostriction and inverse magnetostriction could be mostly explained, as a first approximation, by the rotation of magnetic moments [21]. Generally, in a magnetostrictive specimen, numerous magnetic domains exist, each having a local magnetization while the total magnetization of the material is the sum of each local contribution. As depicted in Figure 1, in the initial state, all the domains are assumed to be randomly distributed, yielding a null magnetization. In an energy harvesting process, the application of a bias magnetic field first leads to a rotation of magnetic moments [22] following the magnetic force and makes the sample longer. When a tensile stress is superimposed along the same direction, the sample becomes elongated, and the magnetic domain continues rotating. This external tensile stress is imposed through mechanical excitation. The magnetic flux in the specimen then varies with the rotation of the magnetic domains.

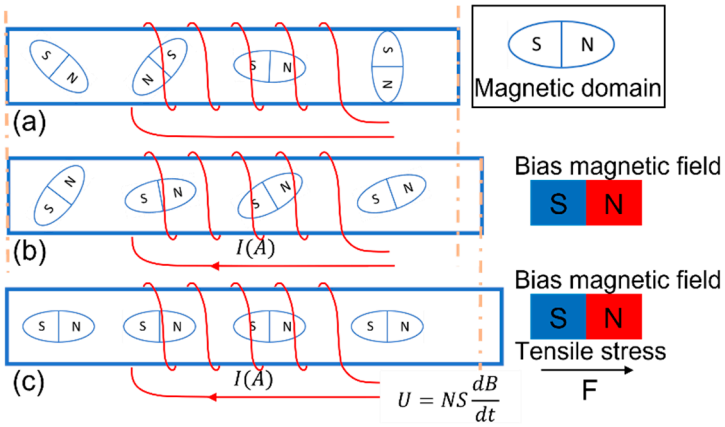


Figure 1. Mechanisms during the process of magnetization. (**a**) Sample in initial state, (**b**) Sample in the bias magnetic field, (**c**) Sample in the bias magnetic field under tensile stress.

Materials such as Terfenol-D [23] and Galfenol [24] have been extensively used in magnetostrictive energy harvesters, along with Fe–Co alloys [25] and Metglas 2605SA1 [26,27] to some extent. Terfenol-D and Galfenol are among the materials with the highest energy conversion potential and are commercially available [28]. Terfenol-D is brittle under tension [29] but shows higher admissible compressive stress around 300–880 MPa [30]. Hence, this material is usually used in harvester systems in the shape of rods and mainly works under compressive stress. Galfenol is usually used in unimorph or bimorph cantilevers. However, the costs of Galfenol and Terfenol-D remain too prohibitive for them to be considered realistic constituents of energy harvesters aiming at replacing batteries.

Hence, the question behind the actual and realistic use of magnetostrictive materials as microgenerators lies in finding a cost-effective solution with decent performance.

As listed in Table 1, Metglas 2605SA1 is a soft magnetic material saturating at 500 A/m with a magnetostrictive coefficient of 41 ppm [31], both being much lower than Galfenol and Terfenol-D. However, its much lower price, around 100 EUR/kg [32] compared to 10,000–20,000 EUR/kg for Terfenol-D and 5000–10,000 EUR/kg for Galfenol [33], makes the mass production and cost-effectiveness possible with respect to battery-powered solutions. To be considered as a conversion material, the intrinsic conversion abilities of such materials should be investigated independently of the structure. Therefore, the conversion ability of Metglas 2605SA1 was measured experimentally and estimated by a biphasic model in this study. Then, Ericsson cycles [34] were assessed on Metglas 2605SA1 foils under different stresses. The Ericsson cycle, in the case of magnetostrictive energy harvesting process, includes two constant stress paths and two iso-magnetic field paths. The constant stress path can be simplified to the unipolar anhysteretic BH curves in this study as explained in Section 3. Therefore, it can easily be assessed from magnetic characterization and models, while being quite easy to achieve experimentally. The Ericsson cycle can also give a formal and clear basis for comparison purposes in terms of energy conversion abilities, as the area enclosed by the cycle represents the converted energy under a given stress level and magnetic conditions.

Table 1. Characteristics of different magnetostrictive materials used for energy harvesting.

Materials	Magnetostriction	Saturation Magnetic Field	Range of Bias Magnetic Excitation	Price 1000 EUR/kg
Galfenol	400 ppm [35]	20 kA/m	3.58 kA/m [36] 40 kA/m [37]	5–10 [33]
Terfenol-D	1100 ppm [38]	10 kA/m	24 kA/m [28]	10–20 [33]
Metglas 2605SA1	41 ppm [31]	0.5 kA/m	<1 kA/m [39]	0.1 [32]

In this work, the experimentally measured energy densities obtained by performing the Ericsson cycle were compared with the predicted results from a dedicated model to evaluate the energy conversion capabilities of Metglas 2605SA1. Results confirmed the validity of the model along with the relevance of Metglas for energy harvesting applications. We also give the orders of magnitude of the converted energy density under various excitation magnetic fields and applied mechanical stresses, yielding insights with respect to conventionally used materials. The paper is organized as follows: Section 2 describes the experimental methods for determining the magnetic properties, and Section 3 gives the energy conversion using Ericsson cycles, followed by the conclusions.

2. Magnetic Behavior

As a first step towards the investigation of the energy conversion abilities of Metglas, this section aims at assessing the magnetic responses of the considered material, along with the development of a theoretical framework to predict the energy conversion performance. Starting from the experimental characterization of Metglas 2605SA1, a model is thus proposed to predict the ultimate energy conversion capability.

2.1. Experimental Setup

The variation of the magnetic flux density (B) when applying an excitation magnetic field (H) was measured with a dedicated test bench. Measurements under several constant tensile and compressive stresses were performed. The schematic of the setup is shown in Figure 2. The magnetic excitation part was composed of two U-shaped yokes, the considered sample, and two coils. The U-shaped yokes ensured the closing of the magnetic circuit to maximize the magnetic flux density in the sample. The primary coil of 110 turns

was wound on the two yokes separately and equally (55 turns each) and ensured the generation of the magnetic excitation from an electrical input. A sinus excitation voltage was generated by a waveform generator (TEKTRONIX AFG1062) and amplified through an amplifier (YOKOGAWA 7058). To obtain the value of the current in the primary coil (and thus the applied magnetic excitation level), a resistance of 20 Ω was connected in series with the coil. A second sensing coil of 500 turns was also wound around the Metglas 2605SA1 sample to measure the induced magnetic flux density in the material through the coil voltage using an acquisition system (DEWESoft SIRIUSi). From the measured current through the resistance and the voltage across the sensing coil, the magnetic excitation H and flux density B could be derived from Equations (1) and (2), where N_P and N_S, respectively represent the number of turns of the primary coil and the number of turns of the sensing coil, I the current through the primary coil, l the length of the sample, S the cross-section of the sample, and U the voltage measured across the sensing coil.

$$H = \frac{N_P I}{l} \tag{1}$$

$$B = \frac{1}{N_S S} \int U dt \tag{2}$$

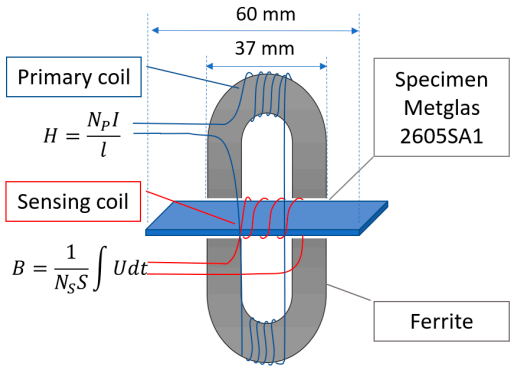


Figure 2. Main circuit of the measurement setup.

In the case of tensile stress, the complete structure of the tensile setup is depicted in Figure 3. The sample consisted of five layers of 25 µm thick Metglas 2605SA1 foil cut with dimensions of 13 mm × 60 mm and glued together with acrylic resin leading to a much lower cross-section than that of the yoke (37 mm × 13 mm), in order to reduce the magnetic flux leakage. The mechanical stress was applied equally on both sides of the sample through cables. The application of the displacement was carried out using actuators (MISUMI RSDG306) that were controlled by MATLAB simultaneously through a dedicated controller (MISUMI EXRS-C1). This displacement was then converted into tensile stress by the cables. A force sensor (RS Pro 204-2773) was connected with a strain gauge converter (WACHENDORFF Z-SG, Italy) to measure the real time mechanical input. In this study, the magnetic characteristics under tensile stress of 0 MPa, 6 MPa, 18 MPa and 30 MPa (corresponding to 0 N, 10 N, 30 N and 50 N, respectively) were recorded.

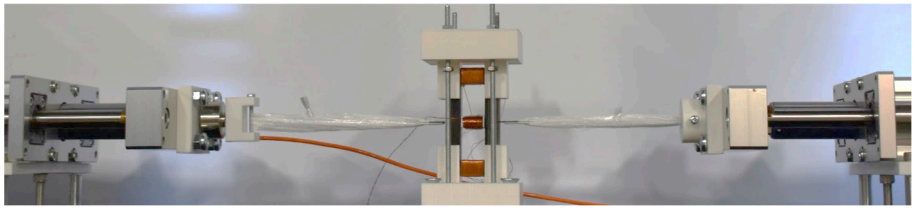


Figure 3. Setup for the measurement of Metglas 2605SA1 under tensile stress.

This setup was also used for measuring magnetic hysteresis response curves under compressive stress as depicted in Figure 4. This was achieved through slight modifications of the tensile testbench by adding 3D printed components, springs, and linear guides. The linear guides were added to ensure that the forces on both sides are on the same horizontal line. Two 3D printed cylinders were added between the sample and the linear guides to isolate the magnetic field. The addition of the springs allows the displacement of the actuators to be converted into the corresponding compression. In the compressive case, the characterization is performed under the same but opposite force, i.e., 0 MPa, −6 MPa, −18 MPa, and −30 MPa, with the positive and negative sign denoting the tensile and compressive stress application, respectively.

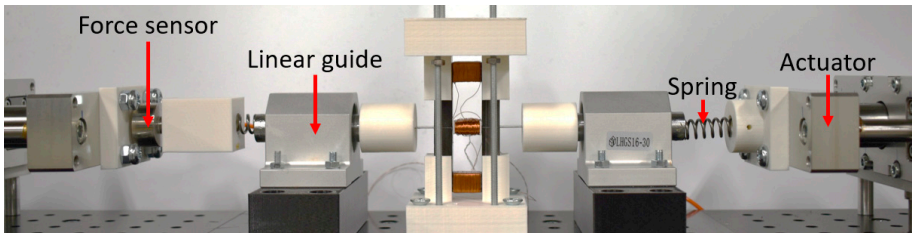


Figure 4. Setup for the measurement of Metglas 2605SA1 under compressive stress.

2.2. Result and Discussion

Firstly, the anisotropy of Metglas 2605SA1 was assessed. The sample denoted "A" was cut in RD (rolling direction) and the one denoted "B" in TD (transverse direction). Both samples were made of a single layer, which increased the stress level to 60 MPa. The characterization result presented in Figure 5 showed a negligible anisotropy. Therefore, the sample mentioned in the following discussion is the sample cut in RD.

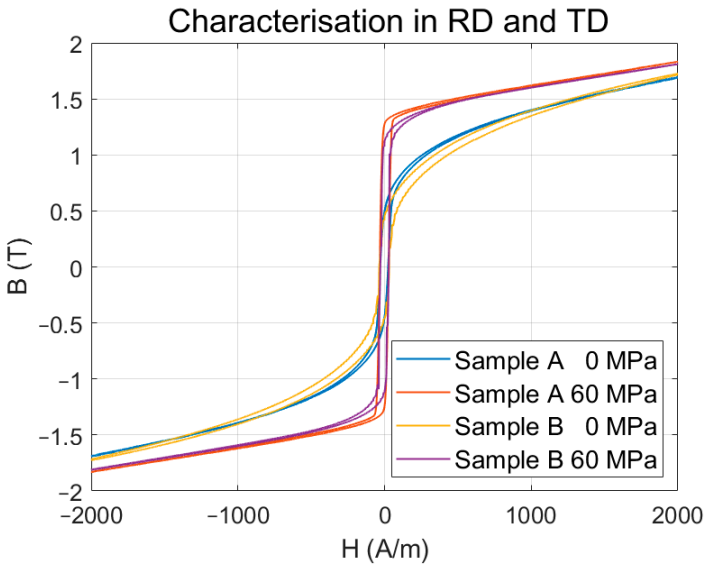


Figure 5. Tensile stress influence on characterization of sample A (rolling direction) and sample B (transverse direction).

The measurements of magnetic hysteresis curves of Metglas 2605SA1 under different compressive and tensile stresses are depicted in Figure 6. These results demonstrate that the coercive field showed low sensitivity to the tensile stresses, and, considering the range of applied magnetic excitation field, could be considered negligible. The results also highlight that the hysteresis behavior has a limited impact on the enclosed area between two curves corresponding to different stresses. Overall, the Metglas experiences a very

limited hysteresis effect over the full stress range. Therefore, the hysteresis effect of the materials is ignored in the following discussion.

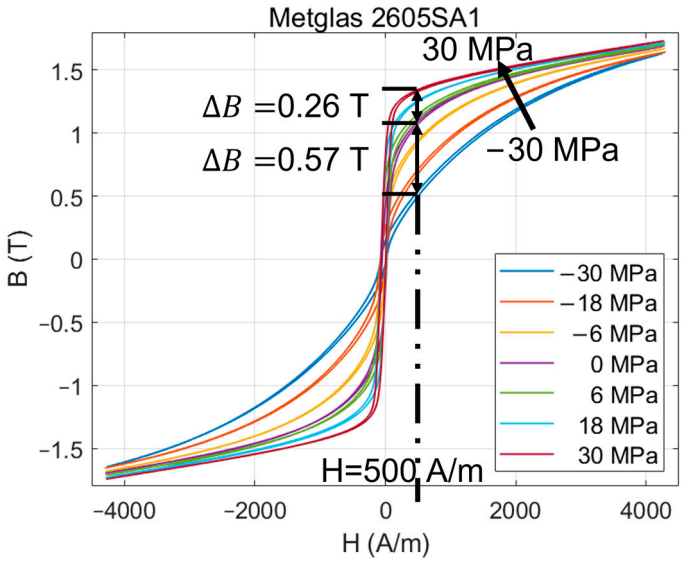


Figure 6. Magnetic hysteresis curves under five tensile stresses.

It could be noted that Metglas 2605SA1 showed a non-negligible linear part in the considered magnetic excitation range. In particular, the tensile stress increased the slope around zero flux density point while the compressive stress apparently decreased the slope. To put it another way, the elongation (resp. contraction) of the sample yielded an increase (resp. decrease) of the low-regime permeability, in accordance with the physical mechanisms behind magnetostriction. This low-field equivalent permeability thus ranged from $600\mu_0$ for a stress of -30 MPa to approximately $8000\mu_0$ for 30 MPa. At zero stress, this permeability was around $5000\mu_0$. As shown in Figure 6, at the same magnetic field level, the induced magnetic flux variation caused by compressive stress was twice that of the one caused under tensile stress. Hence, in terms of relative variation, compressive stress showed higher magnetostrictive activity than tensile stress. Therefore, the effect of stress on the variation of magnetic flux density is not linear, which has also been observed in other materials such as FeCo-2V [40] and FeSiNO [40].

While strong nonlinearity in the form of the hysteresis effect is not considered, as it could be considered negligible, soft nonlinearities arose as the magnetic responses started saturating above 500 A/m. Similarly, the application of tensile stress tended to widen the range of excitation field where the response can be considered linear. Such a behavior is again consistent with the previously exposed physical effects, as application of tensile (resp. compressive) stress yields a rotation of magnetic domains so that they are in the same (resp. perpendicular) axis as that of the applied field. Yet, no clear and pronounced saturation was observed in the range of the excitation field of interest. Unsurprisingly, the results also demonstrate a trade off between low-excitation field equivalent permeability and the wideness of the linear zone. Noticeably, the magnetization tended to converge for all mechanical stresses for excitation fields around 4 kA/m. While such results are qualitatively predictable, as the fully saturated magnetic state is independent from mechanical excitation, these results give relevant quantitative considerations for practical application. Indeed, this results in a closed Ericsson cycle, so that the ultimate energy density under a constant stress would not change even with a higher stress level. Therefore, for Metglas 2605SA1, a higher magnetic field than 4 kA/m is unnecessary.

From these measurements and observations, a model was developed as this investigation focuses on the characterization and prediction of energy density under different stress levels. Among the available modeling possibilities and considering the material characteristics (effect of stress and negligible hysteresis among others), we consider a simplified

anhysteretic model based on a thermodynamic approach presented by Agayan in [41] to relate the magnetic behavior of the considered material. This model focuses more on a mathematical formulation rather than a phenomenological approach, which allows describing the physical meaning of each variable as well as highlighting potential interconnections in the different physical mechanisms. Furthermore, due to the soft magnetic behavior of the Metglas 2605SA1, a biphasic function with an inverse hyperbolic tangent and a linear part is used to describe the sigmoid curves. Therefore, a model that unifies the compressive and tensile excitation is proposed. This biphasic unified model is defined as follows:

$$B = \left\{ \sum_{i=1}^{2} \alpha_i \frac{2}{\pi} \arctan[\beta_i H((1 + \tan h(\gamma_i \cdot \sigma))] \right\} + (\mu - \kappa \cdot \sigma) H \quad (3)$$

where α_i represents the saturation magnetic flux density of a single phase, β_i the small-signal slope of the nonlinear part for the considered phase ($2\alpha_i\beta_i/\pi$ thus being the linear permeability of the corresponding nonlinear phase i under zero stress), μ the zero-stress permeability of the linear part, and γ_i and κ are the magnetostrictive coefficients of the nonlinear and linear phases, respectively. As Metglas 2605SA1 shows a soft saturation at a low magnetic field, two functions of B were combined (biphasic model, $i = 1 \ldots 2$). Each phase can relate different magnetization mechanisms or different magnetization dynamics, for example, arising from domains of different sizes. Based on previous experimental measurements for Metglas 2605SA1, a curve fitting process was carried out. When separating tension and compression cases, a dedicated parameter set was defined for each case, considering the soft nonlinearity (i.e., saturation) on the magnetic flux variation. This model provides a precise prediction for both cases as shown in Figure 7. The corresponding parameters of the model separating tensile and compressive stress are given in Table 2. However, separating compressive and tensile cases would yield a loss in the physical significance of the parameters and in terms of the simplicity of the model. Therefore, the parameters of another fitting process considering a model taking into account both tension and compression conditions are also given in Table 2 and presented in Figure 7. It can be noticed that both models give very similar results and are in good agreement with experimental measurements. Because of its better physical significance and good agreement with experiments, the unified model is considered in the following.

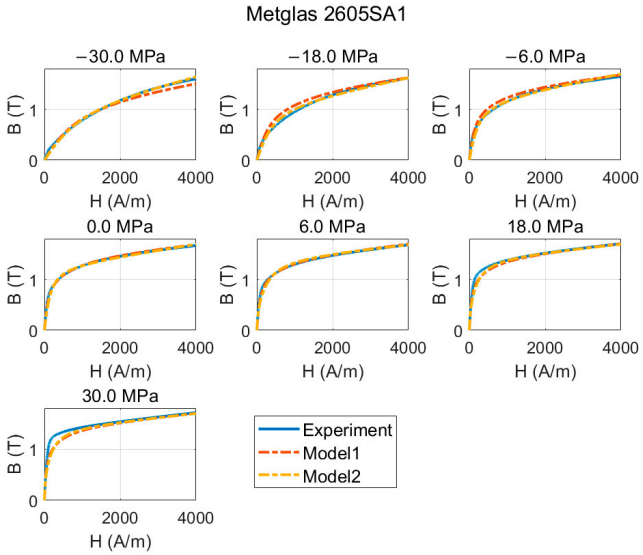


Figure 7. Comparison between anhysteretic curves, common model (Model 1), and the model separating tensile and compressive cases (Model 2) for Metglas 2605SA1.

Table 2. Parameters of the model separating tensile and compressive stress and the common model.

Model	**Separated Model (Tensile)**		**Separated Model (Compressive)**		**Unified Model**	
Phase	***i* = 1**	***i* = 2**	***i* = 1**	***i* = 2**	***i* = 1**	***i* = 2**
α (T)	0.4997	0.9375	0.1741	1.091	0.4464	0.9991
β (m·A^{-1})	24.9×10^{-3}	2.6×10^{-3}	10.6×10^{-3}	6.8×10^{-3}	1.227×10^{-3}	11.04×10^{-3}
γ (Pa^{-1})	3×10^{-8}	4.99×10^{-8}	27.95×10^{-8}	3.765×10^{-8}	2.940×10^{-8}	4.329×10^{-8}
μ (T·m·A^{-1})	7.253×10^{-5}		11.33×10^{-5}		7.817×10^{-5}	
κ (T·m·A^{-1}·Pa^{-1})	7.305×10^{-15}		1.879×10^{-12}		1.566×10^{-13}	

Considering the equivalent low-field permeability μ_{lin} derived from Equation (3) as:

$$\mu_{lin} = \left\{ \frac{2}{\pi} \sum_{i=1}^{2} \alpha_i \beta_i [1 + \tan \mathrm{h}(\gamma_i \cdot \sigma)] \right\} + (\mu - \kappa \cdot \sigma) \quad (4)$$

the theoretical low field equivalent permeability value was found to be $5900\mu_0$, $900\mu_0$, and $10{,}000\mu_0$ for the respective cases of stress free, compressive (−30 MPa), and tensile (30 MPa) stresses, respectively. Such values are in quite good agreement with the previous measurements, preliminarily confirming the relevance of the model. Additionally, the saturation magnetic flux density, given as $\alpha_1 + \alpha_2$, equals 1.45 T, being also in the right range of magnitude of experimentally observed maximal flux density.

Further investigations on the model consisted of assessing the response over the full considered magnetic excitation range. Modeling results and comparisons with experiments are depicted in Figure 7 for Metglas 2605SA1. As previously noted, the experimental magnetic flux density as a function of the magnetic excitation ($B(H)$ curves) shows a limited hysteretic behavior, confirming the anhysteretic modeling approach. It can be noted that the unified model encompassing both tensile and compressive stresses could fit well with the experiment results, not only for the linear part in the low magnetic field range but also considering the saturation part for higher magnetic field levels. Finally, a good agreement between experimental and modeling results can also be observed as the stress is varied, although some slight discrepancies can be observed in the mid-field region at the maximal tensile stresses of 18 MPa and 30 MPa, as well as for −18 MPa compressive stress, and at high excitation values for the maximal tensile stress value of −30 MPa. However, these discrepancies are rather limited, so that the proposed unified model provides a relevant theoretical framework for the energy conversion ability assessment of Metglas.

3. Energy Harvesting Application

Based on the previous measurements on Metglas 2605SA1 and the general theoretical framework exposed in the previous section, this part proposes to investigate the energy conversion potential of such a material for energy harvesting applications using Ericsson cycles.

3.1. Principles of the Energy Harvesting Process

The estimation of the harvestable energy is based on Ericsson-like thermodynamic cycles depicted in Figure 8, with iso-field (D-A, B-C) and iso-stress (A-B, C-D) steps. For an Ericsson cycle [42] considering compressive stress, in initial state A, the specimen is left in an initial state with no magnetic excitation field and no stress, then the magnetic field is increased to state B (without stress). Afterwards, the stress is reduced to state C at constant excitation field, and finally, the magnetic field is decreased back to state D. Then, the removal of the stress at the zero-excitation field leads back to state A. For an Ericsson cycle considering tensile stress, the same process is performed in the order of A-E-F-B-A. During the tensile process, the tensile stress is first increased (A-E), then the magnetic field

is increased to its maximum value at the constant stress level (E-F), after that, the stress comes back to the initial level (F-B), and finally the magnetic field is decreased to the initial state A. Both processes lead to cycles in a clockwise direction, denoting the mechanical-to-magnetic energy conversion process. The theoretical ultimate converted energy from the material produced in this process could be described mathematically by the area enclosed in the cycle (shaded part in Figure 8). Therefore, during the process of energy harvesting, the energy could be maximized by combining the tension and compressive stresses, as shown in Figure 8; an Ericsson cycle from −30 MPa to 30 MPa could be performed in the sequence of D-E-F-C-D.

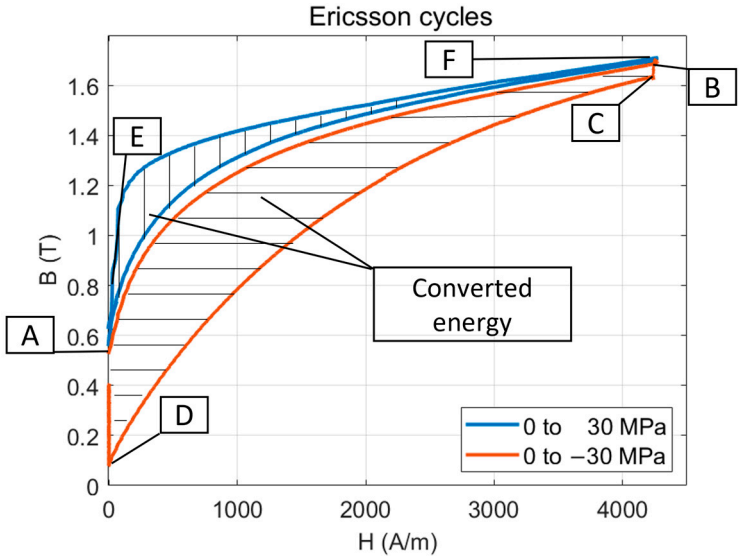


Figure 8. Ericsson cycles of the energy harvesting process under tensile and compressive stress and converted energy density.

3.2. Experiment with Metglas 2605SA1

To experimentally demonstrate the energy harvesting applicability of Metglas 2605SA1 and evaluate the considered model's relevance, the Ericsson-like cycle described in Figure 8 was experimentally implemented. Magnetic excitation consisting of several cycles of square signals (Figure 9a) was considered. The first period was used for assessing magnetic hysteresis curves and estimating the hysteresis losses without stress. The second and third periods actually implemented the Ericsson cycle, as compressive stress was applied to the sample at the maximum magnetic field (transition from state B to state C in Figure 8), and removed when the magnetic field reached a minimum value (transition from state D to state A).

Magnetic hysteresis effect causing energy losses is an important factor in energy calculations. In the case of Metglas 2605SA1, the magnetic hysteresis curves performed a counterclockwise cycle as shown in Figure 9b, denoting hysteresis losses in one unipolar cycle, while the Ericsson cycle formed a clockwise cycle confirming the actual energy conversion process. The small area of the BH curves confirmed that the hysteresis effect could be neglected in the calculation of the harvested energy. The associated area corresponded to the harvestable energy in the latter case. The estimated energy density in one unipolar cycle of Metglas 2605SA1 is presented in Figure 10. This figure confirms that the material has a larger energy density under compressive stress.

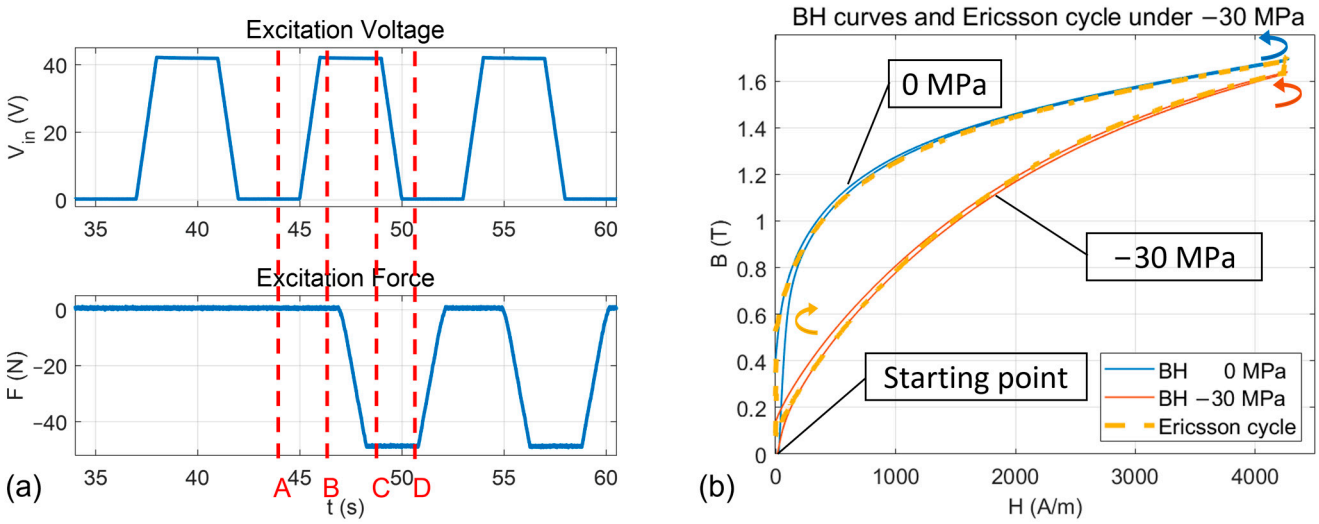


Figure 9. (**a**) Experimental magnetic hysteresis curves and energy harvesting cycle of one unipolar cycle (**b**) Comparison between BH curves and Ericsson cycle.

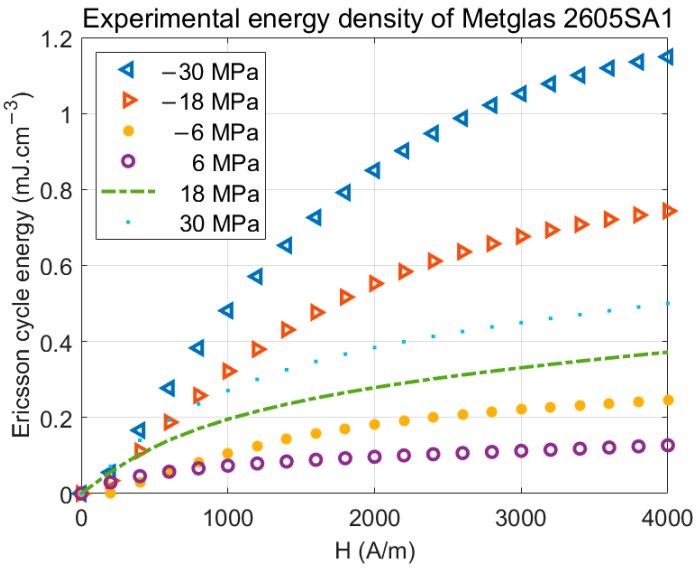


Figure 10. Harvestable energy density estimated from experimental BH curves of Metglas 2605SA1 in a unipolar cycle in the range of 0–4 kA/m.

The developed model was also used to predict the converted energy of the Ericsson cycle. The estimated harvestable energy under different conditions is presented in Figure 11. Furthermore, Table 3 shows the converted energy densities calculated from the experimental Ericsson cycle and the proposed model. The difference between data and model is usually attributed to hysteresis losses, which might not be related to the used model (as the one considered in this work). However, the previous characterization of the Metglas sample revealed a very small hysteresis effect (see Section 2.2), yielding the conclusion that hysteresis does not play a significant role in the difference between predicted and measured energy density values. Instead, it has to be noted that the model of BH curves under different stress levels is fitted with the full bipolar magnetic hysteresis loops. However, the magnetic field is always positive during the measurement of Ericsson cycles. This therefore leads to a partial demagnetization and a smaller magnetic loss than a full cycle. The losses calculated from the bipolar magnetic hysteresis curves under pressure and tensile stress are all in the order of magnitude of 0.1 mJ/cm^3. Therefore, in the case of −6 MPa, even the predicted result of the energy density is in the same order of

magnitude as the magnetic losses, and the harvested energy is still positive. In addition, results indicate that the energy density predicted from the model is in the same order of magnitude as experimental measurements for both the compressive stress and tensile stress. Consequently, it is confirmed that the model could predict correctly the energy harvesting performance.

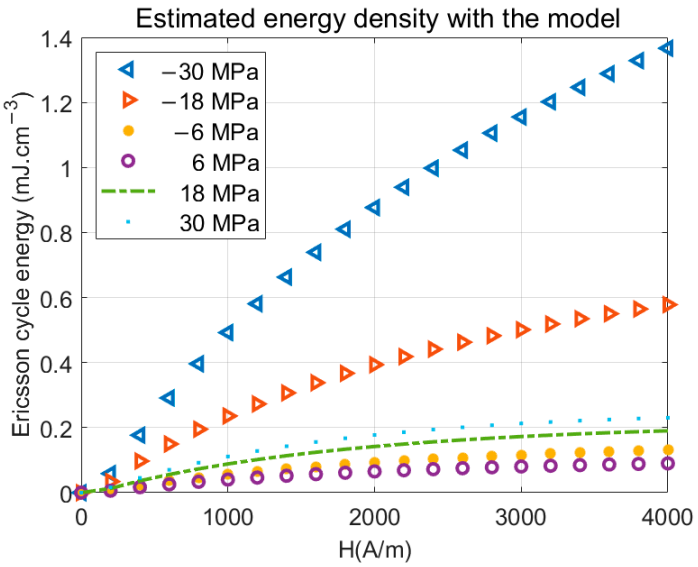


Figure 11. Estimated harvestable energy density of Metglas 2605SA1 in a unipolar cycle with the model in the range of 0–4 kA/m.

Table 3. Experimental validation of the estimated energy density of one unipolar cycle under 4 kA/m.

	mJ/cm^3 (−30 MPa)	mJ/cm^3 (−18 MPa)	mJ/cm^3 (−6 MPa)	mJ/cm^3 (6 MPa)	mJ/cm^3 (18 MPa)	mJ/cm^3 (30 MPa)
Experimental	1.18	0.64	0.19	0.04	0.26	0.29
Model	1.36	0.58	0.13	0.09	0.19	0.23

In numerous reported configurations, the dynamic response around a bias field is considered, and the maximum dynamic excitations of different materials are achieved in a different magnetic field. The energy harvesting is based on a bias magnetic field and small variations around it due to reluctance variations resulting from mechanical stress application or vibrations. Therefore, another important figure of merit lies in the ratio of ΔB over $\Delta\sigma$, denoting the magnetostrictive coupling. In [43], the $\Delta B/\Delta\sigma$ of the devices using Terfenol-D could reach 0.024 T/MPa. In [44], another energy harvesting device using Galfenol has a ratio of 0.034 T/MPa. This value of flux density variation of stress variation for Metglas 2605SA1 is presented in Figure 12. It shows that the optimal condition is achieved around 100 A/m with a ratio reaching nearly 0.015 T/MPa, about 63% of that of Terfenol-D. This figure demonstrates the interest in using Metglas 2605SA1 in a low magnetic excitation zone while Terfenol and Galfenol usually require bias fields higher than 20 kA/m, as shown in Table 1, and therefore bulky magnets bringing a large reluctance to the magnetic circuit. Metglas 2605SA1 is most active at much lower magnetic excitation field, which is consistent with a realistic implementation of magnetostrictive microgenerators in addition to cost-effectiveness.

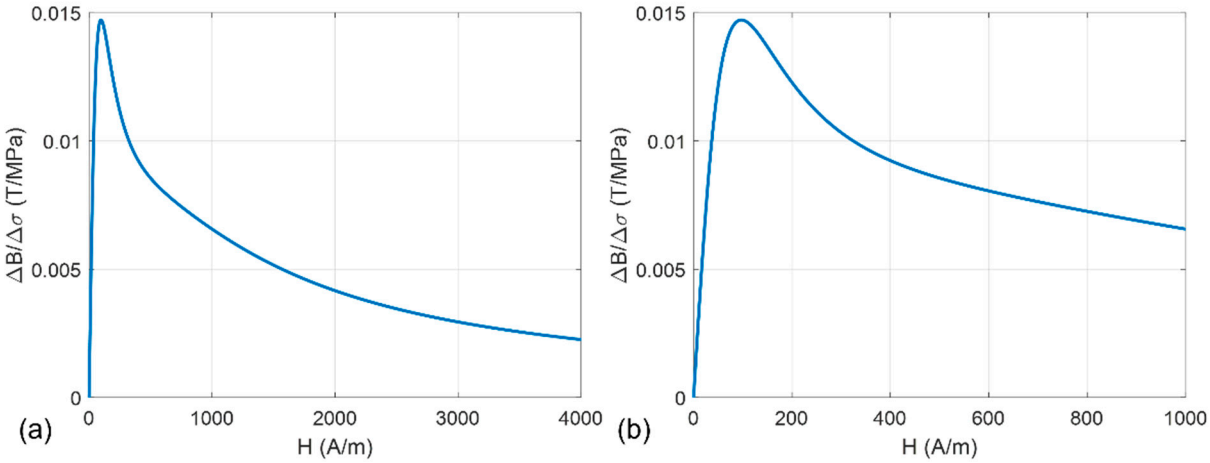


Figure 12. Comparison of variation of $\Delta B/\Delta\sigma$ of Metglas 2605 SA1 with the model (**a**) in the range of 0–4 kA/m and (**b**) zoomed in on the range of 0–1 kA/m.

4. Conclusions

Due to their robustness and potential electromechanical coupling, magnetostrictive materials are a competitive solution for vibrational energy harvesters. Yet, their realistic implementation, mainly due to the material price, as well as the deep understanding of their conversion efficiency, is still an open question.

In this work, an investigation of a magnetostrictive material Metglas 2605SA1 was proposed based on a theoretical framework and experimental data because of its low price (thirty times lower than Galfenol and Terfenol-D) and soft magnetic behavior. The energy conversion capability was assessed under high levels of mechanical stress and excitation fields. Results showed that for low magnetic excitation, which is typical in realistic self-powered implementation using magnets, Metglas 2605SA1 is a premium choice, showing relatively high converted energy in the range of hundreds of $\mu J/cm^3$/cycle through thermodynamic cycles, and reaching up to 1.2 $mJ{\cdot}cm^{-3}$ per cycle for a magnetic field of 4 kA/m and a compressive mechanical stress of 30 MPa. In addition, in the case of low-level energy harvesting under magnetically biased conditions, the magnetoelastic coefficient $\Delta B/\Delta\sigma$ was found to be at maximum under a very low excitation field of 500 A/m, and with a similar value compared to Terfenol-D.

Hence, while not as widely used as a high magnetostriction material, Metglas 2605SA1 appeared to exhibit a very attractive trade-off between cost and performance while being highly suitable in realistic applications using low magnetic excitation.

Author Contributions: Conceptualization, G.S. and M.L.; Methodology, M.L.; Investigation, Y.L., B.D. and G.S.; Data curation, Y.L.; Writing—original draft, Y.L.; Writing—review & editing, B.D., G.S., K.M. and M.L.; Supervision, M.L. All authors have read and agreed to the published version of the manuscript.

Funding: This research received no external funding.

Institutional Review Board Statement: Not applicable.

Informed Consent Statement: Not applicable.

Data Availability Statement: Not applicable.

Acknowledgments: The authors would like to thank Metglas® Inc. for supplying Metglas 2605SA1 materials. This work has been performed in the framework of the MATSURI project of the ELyT Global IRN.

Conflicts of Interest: The authors declare no conflict of interest.

References

1. Ng, I.C.L.; Wakenshaw, S.Y.L. The Internet-of-Things: Review and Research Directions. *Int. J. Res. Mark.* **2017**, *34*, 3–21. [CrossRef]
2. Marin-Garcia, G.; Vazquez-Guzman, G.; Sosa, J.M.; Lopez, A.R.; Martinez-Rodriguez, P.R.; Langarica, D. Battery Types and Electrical Models: A Review. In Proceedings of the 2020 IEEE International Autumn Meeting on Power, Electronics and Computing (ROPEC), Ixtapa, Mexico, 4–6 November 2020; pp. 1–6. [CrossRef]
3. Rani, G.M.; Wu, C.-M.; Motora, K.G.; Umapathi, R.; Jose, C.R.M. Acoustic-Electric Conversion and Triboelectric Properties of Nature-Driven CF-CNT Based Triboelectric Nanogenerator for Mechanical and Sound Energy Harvesting. *Nano Energy* **2023**, *108*, 108211. [CrossRef]
4. Shaikh, F.K.; Zeadally, S. Energy Harvesting in Wireless Sensor Networks: A Comprehensive Review. *Renew. Sustain. Energy Rev.* **2016**, *55*, 1041–1054. [CrossRef]
5. Petsagkourakis, I.; Tybrandt, K.; Crispin, X.; Ohkubo, I.; Satoh, N.; Mori, T. Thermoelectric Materials and Applications for Energy Harvesting Power Generation. *Sci. Technol. Adv. Mater.* **2018**, *19*, 836–862. [CrossRef]
6. Gokana, M.R.; Wu, C.-M.; Motora, K.G.; Qi, J.Y.; Yen, W.-T. Effects of Patterned Electrode on near Infrared Light-Triggered Cesium Tungsten Bronze/Poly (Vinylidene)Fluoride Nanocomposite-Based Pyroelectric Nanogenerator for Energy Harvesting. *J. Power Sources* **2022**, *536*, 231524. [CrossRef]
7. Zhao, J.; Ghannam, R.; Htet, K.O.; Liu, Y.; Law, M.; Roy, V.A.L.; Michel, B.; Imran, M.A.; Heidari, H. Self-Powered Implantable Medical Devices: Photovoltaic Energy Harvesting Review. *Adv. Healthc. Mater.* **2020**, *9*, 2000779. [CrossRef] [PubMed]
8. Wei, C.; Jing, X. A Comprehensive Review on Vibration Energy Harvesting: Modelling and Realization. *Renew. Sustain. Energy Rev.* **2017**, *74*, 1–18. [CrossRef]
9. Deng, Z.; Dapino, M.J. Review of Magnetostrictive Vibration Energy Harvesters. *Smart Mater. Struct.* **2017**, *26*, 103001. [CrossRef]
10. Radousky, H.B.; Liang, H. Energy Harvesting: An Integrated View of Materials, Devices and Applications. *Nanotechnology* **2012**, *23*, 502001. [CrossRef]
11. Kim, H.S.; Kim, J.-H.; Kim, J. A Review of Piezoelectric Energy Harvesting Based on Vibration. *Int. J. Precis. Eng. Manuf.* **2011**, *12*, 1129–1141. [CrossRef]
12. Ando Junior, O.H.; Maran, A.L.O.; Henao, N.C. A Review of the Development and Applications of Thermoelectric Microgenerators for Energy Harvesting. *Renew. Sustain. Energy Rev.* **2018**, *91*, 376–393. [CrossRef]
13. Guyomar, D.; Lallart, M. Recent Progress in Piezoelectric Conversion and Energy Harvesting Using Nonlinear Electronic Interfaces and Issues in Small Scale Implementation. *Micromachines* **2011**, *2*, 274–294. [CrossRef]
14. Narita, F.; Fox, M. A Review on Piezoelectric, Magnetostrictive, and Magnetoelectric Materials and Device Technologies for Energy Harvesting Applications. *Adv. Eng. Mater.* **2018**, *20*, 1700743. [CrossRef]
15. Valadkhan, S.; Morris, K.; Khajepour, A. Review and Comparison of Hysteresis Models for Magnetostrictive Materials. *J. Intell. Mater. Syst. Struct.* **2009**, *20*, 131–142. [CrossRef]
16. Platt, S.R.; Farritor, S.; Haider, H. On Low-Frequency Electric Power Generation with PZT Ceramics. *IEEE/ASME Trans. Mechatron.* **2005**, *10*, 240–252. [CrossRef]
17. Joule, J.P. XVII. On the Effects of Magnetism upon the Dimensions of Iron and Steel Bars. *London Edinb. Dublin Philos. Mag. J. Sci.* **1847**, *30*, 76–87. [CrossRef]
18. Bieńkowski, A.; Kulikowski, J. The Magneto-Elastic Villari Effect in Ferrites. *J. Magn. Magn. Mater.* **1980**, *19*, 120–122. [CrossRef]
19. Zhao, X.; Lord, D.G. Application of the Villari Effect to Electric Power Harvesting. *J. Appl. Phys.* **2006**, *99*, 08M703. [CrossRef]
20. Dapino, M.J.; Smith, R.C.; Faidley, L.E.; Flatau, A.B. A Coupled Structural-Magnetic Strain and Stress Model for Magnetostrictive Transducers. *J. Intell. Mater. Syst. Struct.* **2000**, *11*, 135–152. [CrossRef]
21. Olabi, A.G.; Grunwald, A. Design and Application of Magnetostrictive Materials. *Mater. Des.* **2008**, *29*, 469–483. [CrossRef]
22. Evans, P.G.; Dapino, M.J. Efficient Magnetic Hysteresis Model for Field and Stress Application in Magnetostrictive Galfenol. *J. Appl. Phys.* **2010**, *107*, 063906. [CrossRef]
23. Dai, X.; Wen, Y.; Li, P.; Yang, J.; Zhang, G. Modeling, Characterization and Fabrication of Vibration Energy Harvester Using Terfenol-D/PZT/Terfenol-D Composite Transducer. *Sens. Actuators A Phys.* **2009**, *156*, 350–358. [CrossRef]
24. Yang, Z.; Tan, Y.; Zu, J. A Multi-Impact Frequency up-Converted Magnetostrictive Transducer for Harvesting Energy from Finger Tapping. *Int. J. Mech. Sci.* **2017**, *126*, 235–241. [CrossRef]
25. Yang, Z.; Kurita, H.; Onodera, R.; Tayama, T.; Chiba, D.; Narita, F. Evaluation of Vibration Energy Harvesting Using a Magnetostrictive Iron–Cobalt/Nickel-Clad Plate. *Smart Mater. Struct.* **2019**, *28*, 034001. [CrossRef]
26. Tsutsumi, E.; del Rosario, Z.; Lee, C. *Vibration Energy Harvesting Using the Nonlinear Oscillations of a Magnetostrictive Material*; Sodano, H.A., Ed.; SPIE: San Diego, CA, USA, 2012; p. 834104. [CrossRef]
27. Wang, L.; Yuan, F.G. Vibration Energy Harvesting by Magnetostrictive Material. *Smart Mater. Struct.* **2008**, *17*, 045009. [CrossRef]
28. Staley, M.E.; Flatau, A.B. *Characterization of Energy Harvesting Potential of Terfenol-D and Galfenol*; Flatau, A.B., Ed.; SPIE: San Diego, CA, USA, 2005; p. 630. [CrossRef]
29. Rodríguez, C.; Rodriguez, M.; Orue, I.; Vilas, J.L.; Barandiarán, J.M.; Gubieda, M.L.F.; Leon, L.M. New Elastomer–Terfenol-D Magnetostrictive Composites. *Sens. Actuators A Phys.* **2009**, *149*, 251–254. [CrossRef]
30. Hou, H.; Finkel, P.; Staruch, M.; Cui, J.; Takeuchi, I. Ultra-Low-Field Magneto-Elastocaloric Cooling in a Multiferroic Composite Device. *Nat. Commun.* **2018**, *9*, 4075. [CrossRef] [PubMed]

31. Jen, S.U.; Liu, C.C.; Lin, H.R.; Chou, S.H. Frequency Dependence of the Magnetostrictive Phenomenon in Metglas ® 2605SA1 Ribbon: A Minor-Loop Case. *AIP Adv.* **2014**, *4*, 127140. [CrossRef]
32. Dexter Magnetic Technologies. Available online: https://dxtmagnetics.com/ (accessed on 26 February 2023).
33. Suzhao A-One Special Alloy Co., Ltd. Available online: https://www.aone-alloy.com/ (accessed on 26 February 2023).
34. Zhang, B.; Ducharne, B.; Gupta, B.; Sebald, G.; Guyomar, D.; Gao, J. Experimental Sea Wave Energy Extractor Based on Piezoelectric Ericsson Cycles. *J. Intell. Mater. Syst. Struct.* **2018**, *29*, 1102–1112. [CrossRef]
35. Clark, A.; Wun-Fogle, M.; Restorff, J.B.; Lograsso, T.A. Magnetostrictive Properties of Galfenol Alloys Under Compressive Stress. *Mater. Trans.* **2002**, *43*, 881–886. [CrossRef]
36. Cao, S.; Wang, X.; Zheng, J.; Cao, S.; Sun, J.; Wang, Z.; Zhang, C. Modeling and Design of an Efficient Magnetostrictive Energy Harvesting System With Low Voltage and Low Power. *IEEE Trans. Magn.* **2018**, *54*, 1–5. [CrossRef]
37. Rezaeealam, B.; Ueno, T.; Yamada, S. Finite Element Analysis of Galfenol Unimorph Vibration Energy Harvester. *IEEE Trans. Magn.* **2012**, *48*, 3977–3980. [CrossRef]
38. Sandlund, L.; Fahlander, M.; Cedell, T.; Clark, A.E.; Restorff, J.B.; Wun-Fogle, M. Magnetostriction, Elastic Moduli, and Coupling Factors of Composite Terfenol-D. *J. Appl. Phys.* **1994**, *75*, 5656–5658. [CrossRef]
39. Yu, Z.; Chu, Z.; Yang, J.; Asl, M.J.P.; Yuan, X.; Yu, Y.; Nie, G.; Qi, H.; Dong, S. A Magneto-Mechano-Electric (MME) Energy Harvester Based on Rectangular Cymbal Structure. *Sens. Actuators A Phys.* **2020**, *316*, 112400. [CrossRef]
40. Mahmoud, R. Measurement and Modeling of Magneto-Mechanical Dissipative Behavior of High Yield Stress Ferromagnetic Materials under Multiaxial Loading: Application for High Speed Generator. Doctoral Thesis, École Normale Supérieure de Cachan—ENS Cachan, Gif-sur-Yvette, France, 2014.
41. Agayan, V. Thermodynamic Model of Ideal Magnetostriction. *Phys. Scr.* **1996**, *54*, 514–521. [CrossRef]
42. Lefeuvre, E.; Sebald, G.; Guyomar, D.; Lallart, M.; Richard, C. Materials, Structures and Power Interfaces for Efficient Piezoelectric Energy Harvesting. *J. Electroceram.* **2009**, *22*, 171–179. [CrossRef]
43. Yan, B.; Zhang, C.; Li, L. Design and Fabrication of a High-Efficiency Magnetostrictive Energy Harvester for High-Impact Vibration Systems. *IEEE Trans. Magn.* **2015**, *51*, 1–4. [CrossRef]
44. Cao, S.; Yang, S.; Zheng, J.; Zhang, L.; Wang, B. An Equivalent Circuit Model and Energy Extraction Technique of a Magnetostrictive Energy Harvester. *IEEE Trans. Appl. Supercond.* **2016**, *26*, 1–6. [CrossRef]

Disclaimer/Publisher's Note: The statements, opinions and data contained in all publications are solely those of the individual author(s) and contributor(s) and not of MDPI and/or the editor(s). MDPI and/or the editor(s) disclaim responsibility for any injury to people or property resulting from any ideas, methods, instructions or products referred to in the content.